A nearly 1.5 millennia long record of North Atlantic climatic forcing recorded in tree-ring growth records from Angstel/Vecht Delta, the Netherlands (1283 BCE-156 CE)

Michiel Arts[1*]

Jos Bazelmans[2,3*]

1 - SEDICLIM lab, Department of Geology, University of Liège, Belgium

2 - Cultural Heritage Agency of the Netherlands and Faculty of Archaeology

3 - University of Leiden, Leiden, Netherlands

*These authors contributed equally to this work.

Corresponding Author Email: j.bazelmans@cultureelerfgoed.nl

This manuscript is a non–peer-reviewed preprint submitted to EarthArXiv and is currently under review at The Holocene.

Keywords: tree-ring growth, bog oak, alder carr, Angstel and Vecht, Netherlands, hydroclimate variability, North Atlantic Oscillation (NAO), Atlantic Multidecadal Oscillation (AMO), bicoherence, groundwater dynamics, (cross) wavelet analysis, climate forcing

Abstract

The impact of multi-annual to decadal climatic cycles on tree-ring growth remains understudied. Here, we analyse a nearly one-and-a-half-thousand-year-long tree-ring chronology (1283 BCE–156 CE) based on bog oaks from an alder carr environment in the Angstel-Vecht delta in the Netherlands to assess the influence of multi-year climatic oscillations on tree-ring growth and the origin of the identified cycles. Wavelet, crosswavelet, and bicoherence spectral analyses reveal significant cycles ranging from 2.2 to 100 years. To investigate the forcing mechanisms behind these cycles, we compare the tree-ring record with the Uamh an Tartair stalagmite record from northwestern Scotland, reflecting large-scale variability in North Atlantic precipitation. Cross-wavelet analysis reveals a quarter-cycle phase lag across multiple timescales, indicating a shared North Atlantic climatic driver, with the stalagmite responding almost instantaneously, whereas the Angstel/Vecht tree-ring record shows a delayed response. This delay is attributed to cumulative climate forcing mediated by groundwater changes and hydrological storage processes within the peatland system. The phase relationships suggest that, alongside flooding events, periods of increased regional rainfall elevate groundwater levels, suppressing oak growth in the Angstel/Vecht delta. The 100-, 60-, and 24-year cycles correspond to known climatic oscillations linked to North Atlantic climate modes such as the North Atlantic Oscillation (NAO) and the Atlantic Multidecadal Oscillation (AMO), or possibly solar cycles. Some cycles, such as the 40- and 15-year cycles, cannot be directly attributed to external forcing but instead appear to be nonlinear combination tones. These results indicate that cyclicity in tree-ring growth reflects non-linear interactions among multiple forcing mechanisms across timescales, and demonstrate that lowland wetland bog oak records provide sensitive archives of multiannual to multidecadal hydroclimatic variability in the North Atlantic region over long timescales.

1. Introduction

Hydroclimate variability in Western Europe is strongly influenced by large-scale climate patterns over the North Atlantic, especially the North Atlantic Oscillation (NAO), the Atlantic Multidecadal Oscillation (AMO), and solar cycles (Ait Brahim et al., 2018; Börgel et al., 2020; Dieppois et al., 2013; Lüdecke et al., 2020; Pinto and Raible, 2012). These patterns affect temperature, rainfall, storm activity, and groundwater recharge over seasonal to centennial timescales, leaving clear traces in ocean, lake, and cave records (Ait Brahim et al., 2018; Baldini et al., 2008; Denniston et al., 2008; Hubeny et al., 2006; Rust et al., 2020). However, how these climate patterns are reflected in tree-ring data from lowland areas—especially before the 19th century—remains unclear, making it difficult to identify cycles and nonlinear interactions among different climate influences.

Tree rings provide records of annual hydroclimate variability. In the Angstel/Vecht region of the central Netherlands, oaks grew in alder carrs on peat. Here, groundwater was closely linked to precipitation and discharge from the Rhine River (Jansma, 2020). High rainfall and runoff raised groundwater levels, prolonged anaerobic soil conditions, shortened the growing season, induced root decay, impaired ectomycorrhizal functioning, and increased the risk of oak mortality (Coder, 1994; Copini et al., 2016; Sass-Klaassen and Hanraets, 2006). Drier conditions allowed wider ring increments by improving root conditions (Sass-Klaassen and Hanraets 2006). Both wetter and drier hydrology affect tree growth and mortality. Prolonged high groundwater is suggested to have suppressed germination, depressed growth, and increased mortality. Continued peat formation favoured the preservation of subfossil wood by limiting microbial decay in waterlogged settings (Leuschner et al., 2002; Sass-Klaassen and Hanraets, 2006).

Atmospheric pressure patterns associated with the positive NAO phase are closely linked to major flood events in northwestern Europe (Brönnimann et al., 2025). The NAO index expresses the pressure difference between the Azores High and the Icelandic Low. This difference controls the strength and direction of westerly winds and storm tracks across the North Atlantic (Domeisen et al., 2018; Eade et al., 2022; Folland et al., 2009; Hurrell et al., 1997; Hurrell et al., 2003). During positive NAO phases, conditions are generally mild, wet,

and stormy. Negative phases bring colder, drier, and calmer conditions. These shifts are particularly pronounced in winter. The NAO strongly influences winter and spring discharge in the Rhine River (Steirou et al., 2017). Positive NAO phases correspond to elevated winter discharge due to increased precipitation and earlier snow melt. Negative phases correspond to reduced winter discharge followed by a (late) spring or early summer runoff peak. Variability in the NAO occurs on multi-annual timescales. Multi-decadal to centennial intervals of persistent NAO states are identified in paleoclimatic archives (Baker et al., 2015; Faust et al., 2016; Olsen et al., 2012; Seip et al., 2019). Despite extensive research, reconstructions of long-term NAO variability differ due to uncertainties in age models and limitations in the calibration strength of NAO proxies (Baker et al., 2015).

To clarify how North Atlantic climate variability shapes terrestrial hydroclimate, we analyse a 1.5 millennia-long tree-ring chronology (1283 BCE - 156 CE) from the Angstel/Vecht delta. This chronology represents the most robustly replicated segment ($n \geq 10$) of a larger dataset spanning 1371 BCE–488 CE (NLBOG26) with 90,914 measured rings. Our central goal is to determine if this tree-ring record contains signatures of known atmospheric and solar oscillations and their nonlinear interactions. We use the continuous wavelet transform (CWT), Taner filtering, bicoherence spectral analysis, and the cross-wavelet transform (XWT) to identify dominant periodicities and interactions in tree growth that may be linked to major climate modes and solar forcing.

We use CWT to identify and track dominant cycles in the record. Based on these results, we extract principal cycles using a Taner filter and CWT spectral power to evaluate their persistence. Next, we apply bicoherence spectral analysis to determine the extent to which these cycles are influenced by nonlinear interactions among frequency components. We then isolate and compare subsets of nonlinear signals to those generated from higher-order combinations of cycles, testing whether observed interactions produce new cyclic components. Finally, we assess if the identified variability reflects large-scale North Atlantic forcing by performing cross-wavelet analysis between the Angstel/Vecht record and the Uamh an Tartair stalagmite record. This integrated approach directly quantifies how Angstel/Vecht tree growth responds to climatic oscillations and determines how lowland

wetland tree-ring archives capture hydroclimatic variability linked to ocean-atmosphere dynamics and solar forcing.

2. Paleogeographic setting

The Angstel/Vecht delta, located between the Dutch cities of Amsterdam, Utrecht, and Naarden, and the former Zuiderzee/Lake Flevo, represents a Holocene peat-dominated area at the northern margin of the Rhine delta (Van Asselen et al., 2017; Vos et al., 2020; Weerts et al., 2002)(Figure 1). The area developed on an undulating Late Weichselian coversand surface that became buried beneath Holocene peat, lacustrine and fluvial deposits as groundwater levels rose in response to post-glacial sea-level rise, promoting extensive peat formation across the coastal plain (Bos et al., 2009, 2012; Hijma et al., 2019).

The Angstel/Vecht system developed as a distributary of the Old Rhine from the 12th century BCE onwards. Until the early Middle Ages, the Angstel and Vecht rivers conveyed up to about 10% of the Rhine discharge to the North Sea. This formed a dynamic flood basin with interbedded fluvial, lacustrine, and peat deposits (Van der Woude, 1984; Vos et al., 2020; Weerts et al., 2002). Progressive infilling of peat lakes was followed by the development of levees through repeated overbank deposition of clay-rich sediments. This influenced the spatial distribution of peat facies, with wood peat forming in river-influenced areas and more distal zones characterised by rain-fed peat accumulation (Brouwer et al., 2002; De Lange and Bles, 1963; Poelman, 1966; Van Dinter et al., 2017). These processes further structured the landscape and controlled local drainage patterns (Bos et al., 2009).

Thick peat sequences accumulated across this wetland, supporting alder carrs and scattered oaks. These oaks were sensitive to fluctuations in groundwater levels (Jansma 2020; Sass-Klaassen and Hanraets 2006). Elevated water reduced tree-ring growth by limiting root aeration. Drier phases enabled wider ring increments. This hydrological dependence makes the site ideal for reconstructing past hydroclimate. Subfossil oaks in the peat form the Angstel/Vecht tree-ring chronology NLBOG26, detailed by Bazelmans et al. (submitted). In this setting, the Angstel/Vecht region is a highly sensitive archive of externally forced hydroclimatic variability.

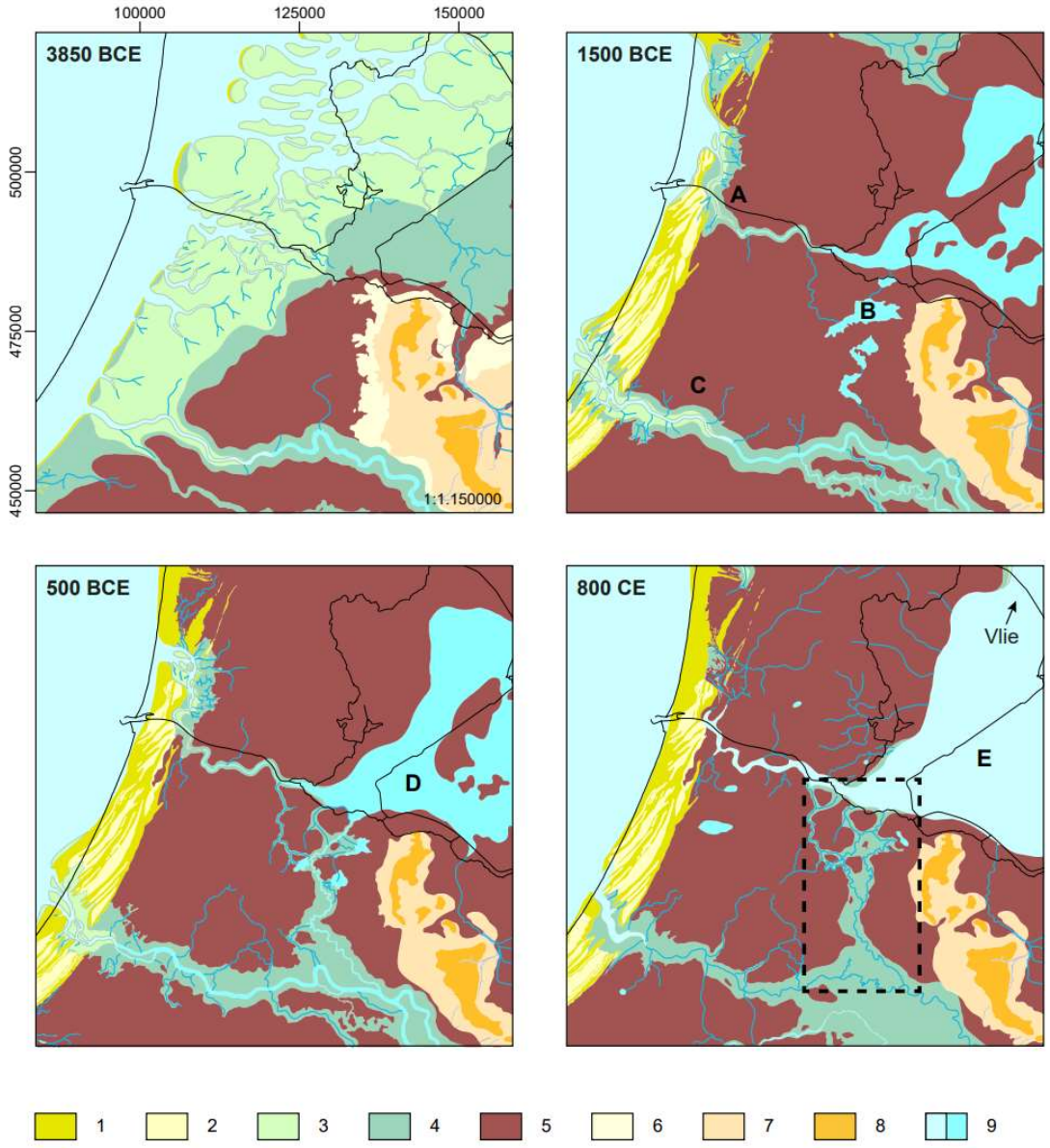

Figure 1. Caption : Figure 1. Palaeogeography of the Angstel-Vecht delta during the 3850 BCE, 1500 BCE, 500 BCE and 800 CE time slices. A, Oer-IJ; B. Lake Aetsveld; C. Old Rhine; D, Lake Flevo; E, Almere. 1, beach barriers and low dunes; 2, beach planes and dune valleys; 3, tidal flats; 4, salt marshes, floodplains and stream valleys; 5, peat areas, 6, Pleistocene sand areas below modern sea level, 7, Pleistocene sand areas above modern sea level; 8, ice-pushed ridges; 9, outer and inner water. Dashed line: research area. Modified after Vos et al., (2018).

3. Materials and Methods

To uncover cyclicity in the Angstel/Vecht tree-ring chronology, we analysed the growth index (GI) record NLBOG26 (Bazelmans et al., submitted; Figure 2, upper panel). This record contains 526 specimens from 31 sites; 500 are absolutely dated and together form a robust chronology for the Angstel/Vecht delta. Raw ring-width measurements include long-term biological trends that can obscure climatic signals. To address this, we used the detrended GI record. We removed age-related growth trends using standard detrending, including a 128-year spline with a 50% variance cut-off (Cook et al., 1990). The calculation was tailored to each time series, using a spline length equal to 67% of the series length, with a maximum spline length of 128 years. We did not consider autocorrelation, as growth is strongly influenced by hydrological factors, and our goal was to detect long-term effects (Jansma, 2020). This processing minimises biological growth effects and retains the climatic signal for spectral analysis (Figure 2, lower panel).

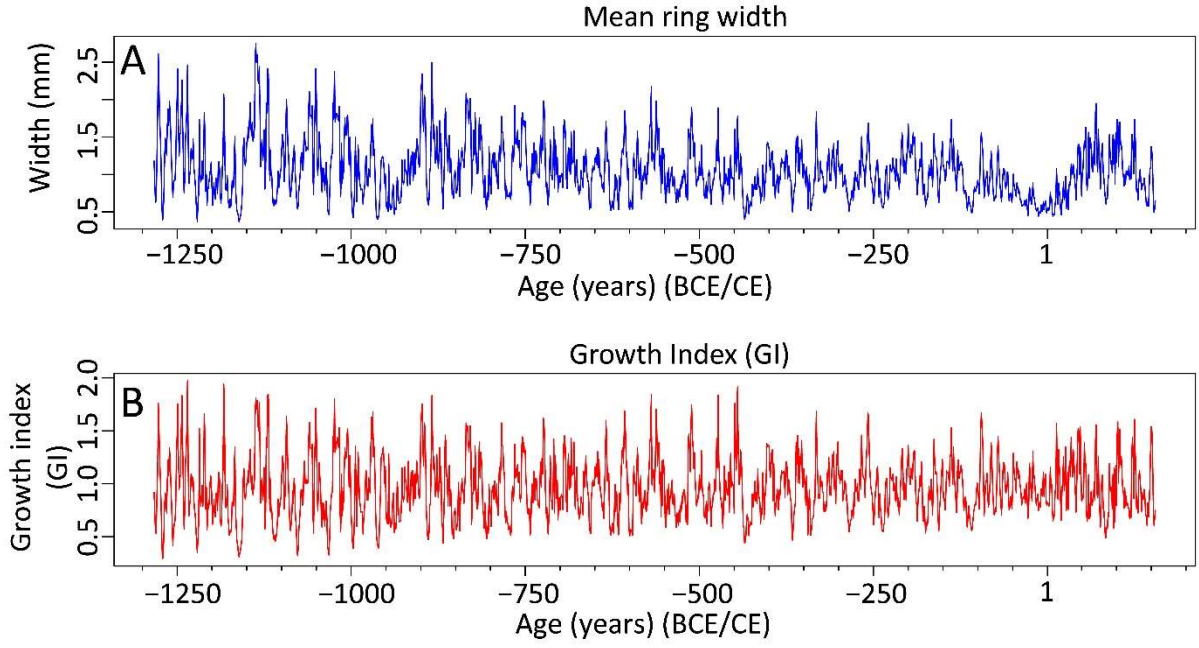

Figure 2. Mean ring with and growth index (GI) records of (Angstel/Vecht) NLBOG26 record of Bazelmans et al. (submitted).

Analyses were performed using functions from the Astrochron (Meyers et al., 2014, 2019) and WaverideR (Arts, 2023; Arts et al., 2024) R packages (see S1 for the R code). The Continuous Wavelet Transform (CWT) and Cross Wavelet Transform (XWT) functions from WaverideR were applied to generate scalograms and examine the temporal variability of cycles. Dominant cycles with high-power spectral peaks were then extracted using the Taner bandpass filter (Taner et al., 2000), as implemented in the Astrochron R package.

Potential nonlinear interactions among higher-order cycles were evaluated using a modified bicoherence function from the Astrochron R package, which employs WOSA-based smoothing to reduce spurious peaks (Choudhury et al., 2008; Hagelberg et al., 1999; Sullivan et al., 2023; Welch et al., 1967). Bandwidth smoothing was applied to obtain reliable estimates, thereby reducing frequency resolution relative to the original power spectrum. Nonlinear components were subsequently extracted from the GI record using a Taner filter to identify combination tones generated by interactions among higher-order cycles.

Finally, to assess whether the detected cycles reflect large-scale North Atlantic forcing, a Cross Wavelet Transform (XWT) was computed between the growth index (GI) record NLBOG26 and the Uamh an Tartair stalagmite growth-rate record from northwestern Scotland (Baker et al., 2015), which is known to capture variability related to the Atlantic Multidecadal Oscillation (AMO) and the North Atlantic Oscillation (NAO) (Baker et al., 2015). This step enables the identification of phase relationships and the evaluation of the regional hydroclimatic significance of the detected cyclicity.

4. Results

4.1 Spectral analysis and cycle extraction

The wavelet scalogram of the Angstel/Vecht chronology reveals spectral peaks with periods of 2.2, 3.6, 5.9, 8, 12, 15.4, 24, 38, 60, 80, 110, and 200 years (Figure 3). This broad spectrum indicates that the Growth Index (GI) was paced by climatic cycles ranging from biannual to centennial cycles.

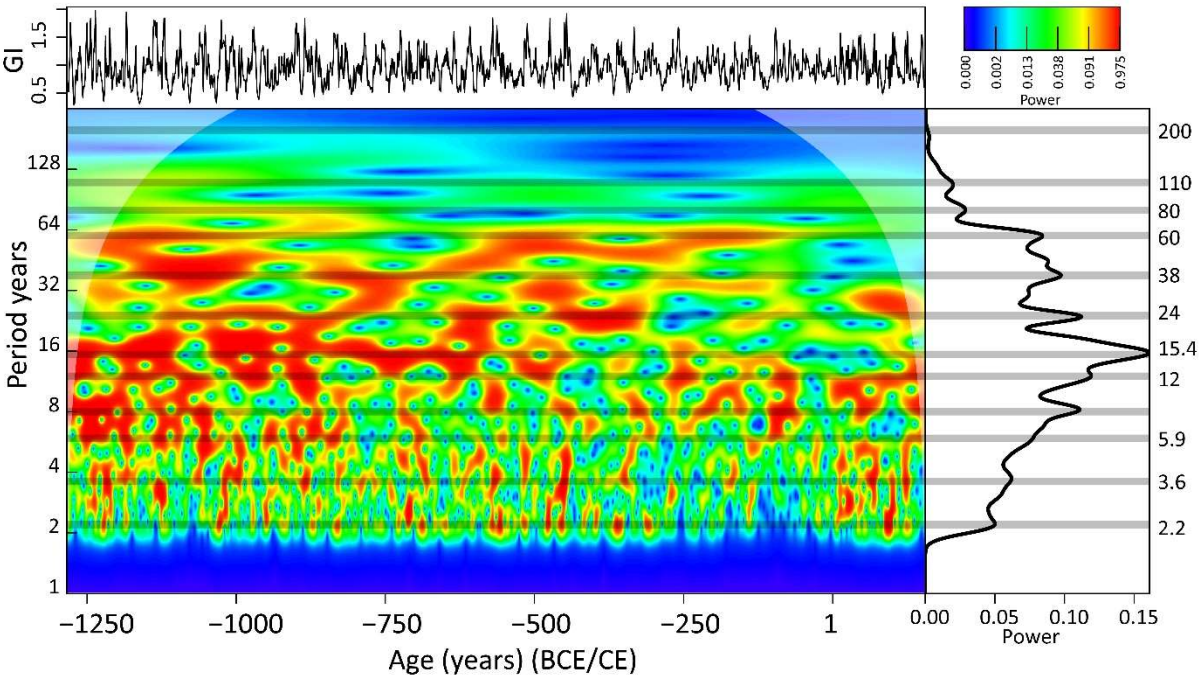

Figure 3. CWT scalogram of the growth index (GI) records of (Angstel/Vecht) NLBOG26 record of Bazelmans et al. (submitted).

To isolate the astronomical signal from the underlying noise, we performed targeted extraction of the most prominent spectral peaks (approximately 3.6, 8, 15, 38, 60, and 110 years) from the GI record (Figures 4A-4F). Lower-amplitude spectral peaks, specifically those at 2.2, 5.9, 12, 24, 80, and 200 years, were excluded from further analysis due to insufficient spectral power and a lack of temporal persistence, especially for the shorter-period cycles. The spectral power of each selected cycle was calculated as a percentage of the total spectral power, quantifying its relative contribution over time (Figure 4G). When plotted alongside the original GI record, the 15.4, 38, and 60-year cycles are clearly evident in the raw data. Conversely, the shorter (3.4 and 8-year) and longest (110-year) components are less visually apparent but still contribute to the overall spectral power.

The relative contribution of each cycle to the total spectral power varies considerably through time (Figure 4G). The ~110-year cycle shows low spectral power, suggesting a minor influence on overall variability. In contrast, the ~60-year cycle dominates the low-frequency domain, accounting for a substantial portion of the spectral power prior to year 1. Cycles of

decadal duration (38 and 15.4 years) exhibit distinct yet intermittent contributions, reflecting periodic but non-continuous modulation. The shorter cycles (~8 and ~3.4 years) exhibit low power and high variability, suggesting they represent high-frequency fluctuations superimposed on longer-term trends. Ultimately, the stacked spectral power distribution reveals a hierarchical organisation of cyclicities within the GI record, characterised by temporal shifts in the dominance of different frequency components.

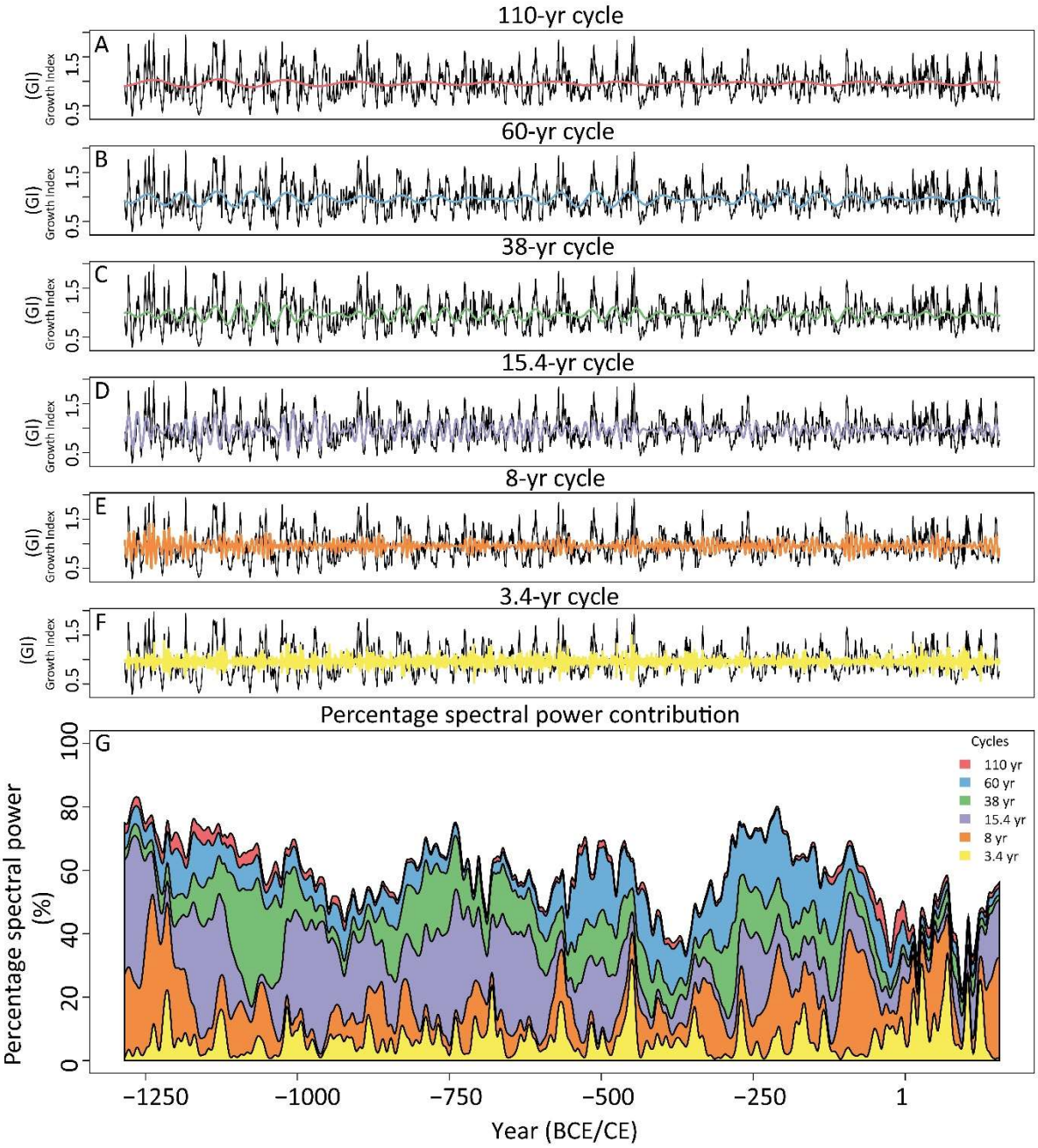

Figure 4. Extracted cycles and spectral power. A GI record and extracted 110-year cycle, B GI record and extracted 60-year cycle, C GI record and extracted 38-year cycle, D GI record and

extracted 15-year cycle, E GI record and extracted 8-year cycle, F GI record and extracted 3.4-year cycle, G extracted the spectral power (CWT) of the different cycles.

4.2 Identifying non-linear interactions via bicoherence analysis

Bicoherence spectral analysis reveals that several shorter-period cycles in the Angstel/Vecht chronology emerge as nonlinear combination tones of longer-period oscillations (Figure 5). Due to the complexity of the bicoherence plot, we have selected the most prominent spectral interactions as representative examples of this nonlinear coupling. Specifically, the interactions between the 110- and 60-year cycles, which generate a ~40-year combination cycle, and the 24- and 40-year cycles, which combine into a ~15-year cycle, are presented as primary examples.

These specific combinations were selected because they exhibit higher spectral power, and the 45-degree dashed line in the figure can clearly be linked to a spectral peak. Furthermore, these two cases result in cycles closely analogous to the 15.4- and 38-year cycles observed in the CWT scalogram (see Figure 3). While other non-linear combinations are observed, they are poorer examples due to their lower power values and less distinct alignments with the primary spectral peaks in the CWT.

To evaluate the interpretations drawn from the bicoherence spectra, we synthesised the daughter components by multiplying the two corresponding higher-order parent cycles to determine if they replicate the observed signal (Figure 6). Specifically, the 60- and 110-year combination-tone cycles were multiplied to generate a 37.5-year daughter cycle, which was subsequently extracted from the record (Figure 6B). A similar procedure was applied to the 24 and 40-year combination tones to isolate the 15-year daughter cycle (Figure 6C). Comparing the generated daughter cycles with those directly extracted from the raw record shows that they are either completely in phase or completely out of phase. This confirms that nonlinear interactions between cycles created new cyclic components that are either completely in phase or out of phase, depending on the complex nonlinear interaction that occurred during the creation of the daughter cycle. The observation of nonlinear behaviour that creates new cyclic components indicates that tree-ring growth variability is shaped by

the interplay of multiple climatic oscillations rather than by the isolated influence of a single climatic mode.

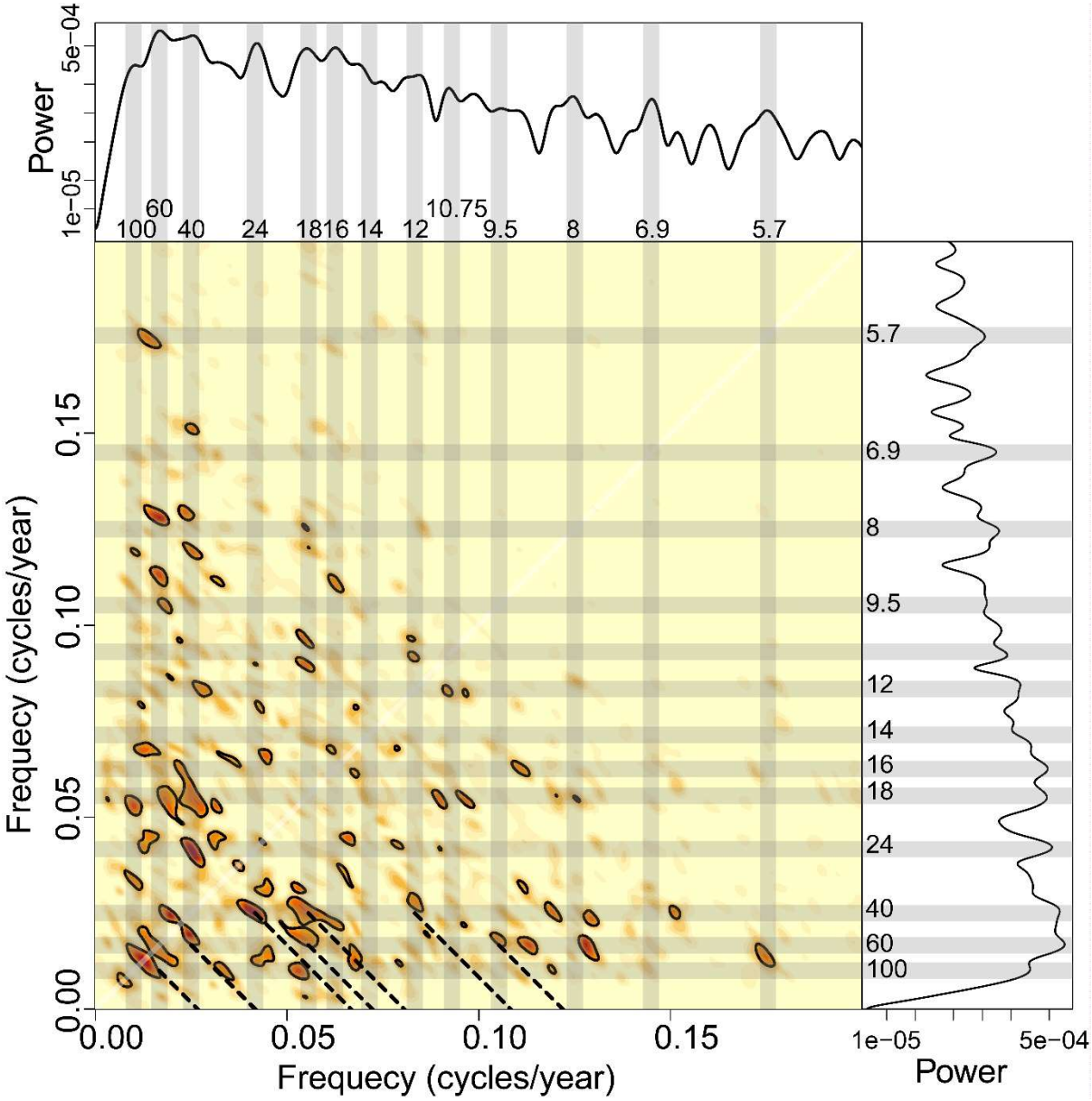

Figure 5. Bicoherence plot of the GI record. The spectral peaks are indicated in the figure. Dashed lines indicate non-linear components interacting to create now cycles and the corresponding astronomical peaks.

4.3 Cross-wavelet comparison with the Uamh an Tartair stalagmite record

To better understand the climatic origins of the cycles in the Angstel/Vecht record, a cross-wavelet analysis was performed against the Uamh an Tartair stalagmite record from Scotland, an archive known to be driven primarily by North Atlantic weather and its resulting precipitation patterns (Baker et al., 2011; Baker et al., 2015; Proctor et al., 2000.

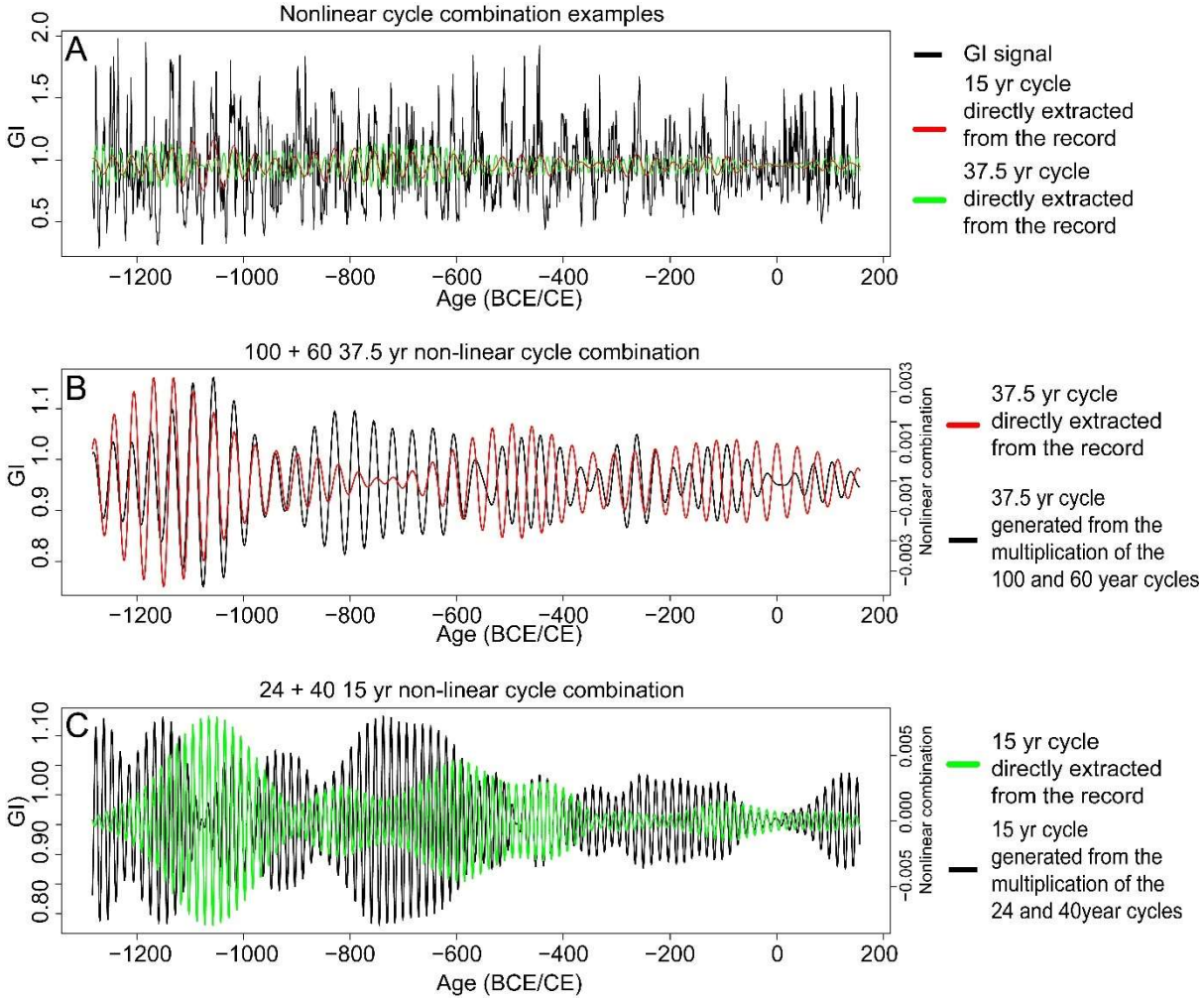

Figure 6. A. The growth index and the 15- and 37.5-yr cycles directly extracted from the record, B. 37.5-yr cycle directly extracted from the record, and the 37.5-yr cycle generated from the 60 and 100-yr cycles, C. 15-yr cycle directly extracted from the record and the 15-yr cycle generated from the 24 and 40-yr cycles.

Cross-wavelet analysis between the stalagmite and bog oak GI records identifies significant shared spectral power across multidecadal to centennial scales. The highest spectral density is concentrated within the 30-60-year periodicities (Figure 7). A Secondary high-power area

is observed between the 30- and 8-year period intervals. In this interval, spectral power is more variable, as is the direction of the phase arrows. Phase arrows in the cross-wavelet plots predominantly point upward (≈90°) or downward (≈270°), with more upward-pointing arrows, indicating a persistent quarter-cycle phase-lag. The phase arrows more or less point either upwards or downwards, regardless of the observed period range, demonstrating that the stalagmite signal consistently leads the bog oak response by a quarter cycle, regardless of cycle length. Consequently, the absolute temporal lag scales with the associated periodicity.

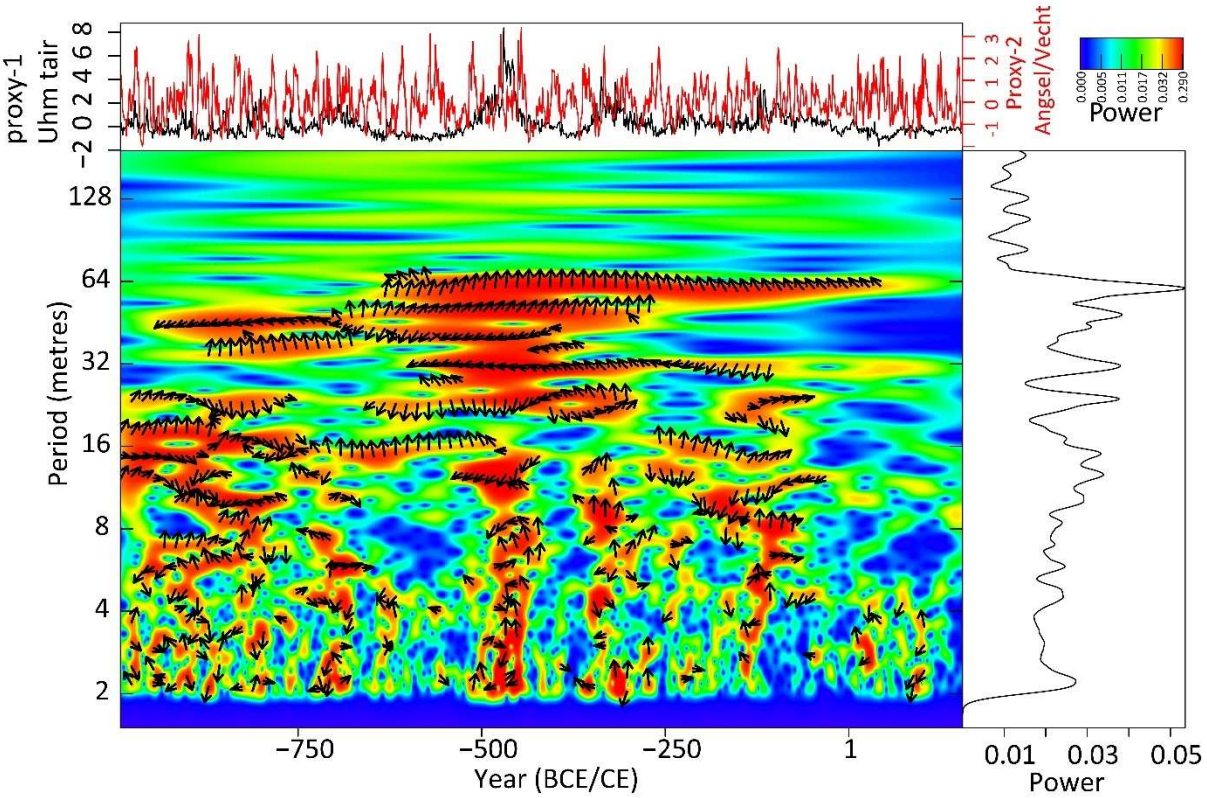

Figure 7. cross-wavelet spectra between the Angstel/Vecht bog oak GI dataset and the stalagmite growth rate dataset from the Uamh an Tartair stalagmite record, Scotland, of Baker et al., 2015.

5. Discussion

5.1 Hydroclimatic Forcing and System Response Mechanisms

Based on our spectral analyses and cross-wavelet comparisons, we can argue that North Atlantic climate variability exerted a persistent influence on hydroclimate and oak growth across decadal to centennial timescales. The prevalent ~90° phase lag observed between the Uamh an Tartair stalagmites and the Angstel/Vecht bog oaks does not reflect a chronological mismatch. Instead, it documents fundamentally different environmental response mechanisms to a shared North Atlantic climatic forcing (Bond et al., 2001; Hurrell, 1995; Olsen et al., 2012; Rust et al., 2020; Schultz et al., 2015).

The Uamh an Tartair stalagmite growth rate primarily reflects changes in precipitation and groundwater recharge in a blanket peat-dominated karst setting (Baker et al., 2015; Proctor et al., 2000). Stalagmite growth is controlled by hydrological flux through the soil-peat column, which governs soil CO2 production, carbonate dissolution, and drip-water supersaturation (Baker et al., 2011; Baker et al., 2015; Proctor et al., 2000). Because the vadose zone above the cave is only several meters thick and the catchment area is small, precipitation changes are transmitted rapidly into the cave system. Consequently, stalagmite growth rates respond quasi-instantaneously to shifts in moisture balance, particularly during the onset of wetter conditions associated with persistent positive NAO phases (Baker et al., 2011; Baker et al., 2015; Proctor et al., 2000). The stalagmite archive, therefore, records the forcing or instantaneous-flux component of hydroclimatic variability.

Conversely, the GI record from the Angstel/Vecht delta partly reflects local groundwater conditions governed by the long-term storage and residence times of water within the vast Rhine drainage basin. Sustained increases in precipitation and meltwater lead to a cumulative rise in groundwater levels across the drainage basin. Because the groundwater response is not instantaneous, it represents an integrated signal of basin-wide processes. This includes not only local rainfall but also seasonal snow and glacial melt from the upper reaches of the catchment (Viviroli et al., 2003). As long as the recharge rate remains positive, groundwater levels continue to rise. Therefore, the lowest GI results not from the peak rainfall rate, but from the cumulative multi-year effect that produces the absolute highest groundwater levels. These high levels suppress oak growth by reducing oxygen availability in the root zone, inducing metabolic stress, and inhibiting nutrient uptake (Rust et al., 2020; Sass-Klaassen and Hanraets, 2006; Vreugdenhil et al., 2006).

This interpretation requires nuance because high-frequency, extreme precipitation and flood events operate on fundamentally different scales than groundwater. Unlike the slow, integrated rise of the water table, these events occur on seasonal or weekly timescales and can trigger near-instantaneous physiological stress in oak growth. These extremes should not be dismissed as stochastic noise; rather, they exhibit distinct periodicities driven by specific phases of the NAO or AMO. Specifically, positive NAO phases and warm AMO states are associated with increased frequency and magnitude of winter floods in the Rhine catchment (Toonen et al., 2016; Scaife et al., 2008). Consequently, these periodic shifts in flood frequency can superimpose a sharp, instantaneous climatic signal onto the broader, long-term integrated groundwater trend.

In dynamical terms, the tree-ring record represents a state-sensitive response to the integral of the forcing variable. Peak groundwater-induced stress is reached only after a prolonged period of moisture surplus. This integrating behaviour, combined with interference from periodic acute floods, explains the persistent but imperfect quarter-cycle lag observed in the Uamh an Tartair stalagmite growth rate record. While the Uamh an Tartair stalagmite growth reacts to climatic change near-instantaneously, the Dutch bog oaks reflect the cumulative effects of that same change. Given that the Uamh an Tartair stalagmite securely records North Atlantic hydroclimate, we can conclude that the Angstel/Vecht bog oaks are driven by the exact same forcing, albeit expressed through a different hydrological filter. The lowland delta environment functions as a non-linear biological integrator, where external climatic forcings are transformed, amplified, or phase-shifted as they cascade through ocean-atmosphere feedbacks before being filtered through the immense hydrology of the Rhine drainage basin (Bond et al., 2001; Hurrell et al., 2003; Olsen et al., 2012; Scaife et al., 2013).

5.2 Linking Cycles to Climatic Patterns

The broad spectrum of periodicities observed in the Angstel/Vecht GI record indicates that lowland oak growth is governed by a hierarchy of interacting climatic patterns, ranging from fast-acting atmospheric oscillations to slow-moving oceanic and solar drivers.

The shortest spectral peaks in the GI record can be coupled to high-frequency atmospheric variability. Periodicities between 2 and 4 years in the Angstel/Vecht record are consistent with the Quasi-Biennial Oscillation (QBO), which modulates stratospheric wind fields and subsequently affects mid-latitude storminess and precipitation (Baldwin et al., 2001; Brönnimann et al., 2016; Oz et al., 2009; Sonett et al., 1992). Cycles between 5.9 and 8 years fall within the characteristic range of the North Atlantic Oscillation (NAO) (Adolph et al., 2024; Appenzeller et al., 1998; Cook et al., 1998; Hurrell, 1995; Luterbacher et al., 2001; Rust et al., 2020, 2022; Wanner et al., 2001). Positive NAO phases enhance westerly airflow, significantly increasing precipitation across northwestern Europe (Knudsen et al., 2011; Sutton and Hodson, 2005). In the Rhine catchment, these NAO- and QBO-driven periodicities dictate the frequency of instantaneous hydrological shocks and extreme winter flood events, which acutely constrain local oak growth (Sass-Klaassen and Hanraets, 2006).

Underlying these high-frequency atmospheric variations are slower, multidecadal-to-centennial modes of 38, 60 and 110 years in the Angstel/Vecht record that reflect internal variability of the Atlantic Multidecadal Oscillation (AMO) (Ait Brahim et al., 2018; Knudsen et al., 2011). The AMO exhibits a characteristic 60-80-year cyclicity with minor components at 35, 85-100, and 110 years (Delworth and Mann, 2000; Enfield et al., 2001; Goldenberg et al., 2001; Gray et al., 2004; Hubeny et al., 2006; Schlesinger and Ramankutty, 1994; Sutton and Hodson, 2005). By modulating North Atlantic sea surface temperatures, the AMO exerts a profound control over continental evaporation and sustained moisture transport into the European interior. Consequently, AMO dynamics drive long-term cumulative groundwater trends that govern the integrated hydrological baseline of the deltaic environment (Baker et al., 2011; Geirsdóttir et al., 2016; Sass-Klaassen and Hanraets, 2006).

These atmospheric and oceanic systems are further paced by exogenous solar forcing. Periodicities at 12, 24, 58, 80, and 110 years in the Angstel Vecht record can be linked to known solar activity cycles and their amplitude-modulating components, including the 11-year Schwabe and 22-year Hale cycles (Brehm et al., 2021; Hathaway, 2015; Land et al., 2020; Miyahara et al., 2009; Murphy et al., 1994; Nintcheu-Fata et al., 2003; Sonett and Finney, 1990). Imperfect period alignment of the 12- and 24-year cycles with solar cycles

411 either reflects a deep-time period shift or reflects the thermal inertia of the oceans and
412 delayed propagation through the atmosphere, which alters the period of the solar signal
413 (Scaife et al., 2013; Seip et al., 2019). Solar forcing shapes regional hydroclimate via
414 atmospheric circulation patterns, including stratosphere-troposphere coupling, which
415 affects the stability of NAO-like pressure patterns (Hathaway and Wilson, 2004; Lohmann et
416 al., 2004; Seidenglanz et al., 2012; Seip et al., 2019).
417
418 While individual cycles can be linked to discrete climatic phenomena, our bicoherence
419 analyses demonstrate that regional hydroclimate arises from nonlinear interactions among
420 climatic cycles (Land et al., 2020; Schultz et al., 2015). Combination tones, such as the 38-
421 year cycle (arising from the non-linear interaction between the 100- and 60-year
422 interactions) and the 15-year cycle (arising from the non-linear interaction between the 24-
423 and 40-year cycles), illustrate that these forcings do not act in isolation. Instead, slow-
424 moving oceanic boundary conditions (AMO) and top-down solar modulation interact to
425 dictate the probability and intensity of high-frequency atmospheric climatic cycles (NAO and
426 QBO).
427
428 Consequently, the spectral architecture of the Angstel/Vecht chronology is not a simple
429 additive record; it captures interacting climatic modes in which multidecadal oceanic and
430 solar trends systematically modulate high-frequency atmospheric dynamics that govern
431 extreme flood events and groundwater recharge in northwestern Europe. This complex
432 interaction explains why the observed spectral peaks in the Angstel/Vecht record
433 sometimes exhibit slight offsets from the pure solar or oceanic cycles that drive them. The
434 clear expression of both individual cycles and their nonlinear interactions is closely tied to
435 the localised sampling strategy of the Angstel/Vecht chronology, which targets a single
436 drainage region and groundwater system within one branch of the Rhine. By minimising
437 spatial averaging, this approach reduced signal attenuation that might have obscured
438 cyclical variability in larger regional composites. At the same time, it highlights a key
439 limitation. Although a shared North Atlantic forcing links the Angstel/Vecht oak record to
440 other archives, such as the Uamh an Tartair stalagmites, site-specific hydrological filtering
441 prevents straightforward one-to-one correlation of individual cycles between records.
442 Hydroclimatic responses, therefore, remain inherently site-sensitive. This raises an

important question: whether the identified nonlinear interactions are broadly transferable across the region or instead reflect local characteristics of the Angstel/Vecht region. Addressing this will require systematic comparisons across contrasting drainage systems, which are essential for determining whether such nonlinear coupling is a fundamental feature of North Atlantic climate dynamics and for understanding how these interactions would have propagated through and are recorded in palaeoclimatological records within the wider Rhine drainage basin.

6. Conclusion

The nearly 1.5-millennia-long Angstel/Vecht bog oak chronology provides a highly sensitive archive of hydroclimatic variability in northwestern Europe, as evidenced by wavelet, cross-wavelet, and bicoherence spectral analyses, as well as Taner filtering. We show that tree growth in this lowland wetland system is governed by a broad spectrum of cyclicities ranging from interannual to centennial timescales, reflecting the combined influence of atmospheric, oceanic, and solar forcing mechanisms.

The identified periodicities closely match known modes of North Atlantic climate variability, including the North Atlantic Oscillation and the Atlantic Multidecadal Oscillation, as well as solar cycles. However, the spectral structure of the tree-ring record is not a simple linear imprint of these external forcings. Instead, bicoherence analysis reveals that a significant portion of the observed variability arises from nonlinear interactions among primary cycles, generating combination tones that contribute substantially to the overall signal. This highlights the importance of considering nonlinear dynamics when interpreting dendrochronological records.

The cross-wavelet comparison with the Uamh an Tartair stalagmite record provides compelling evidence that both archives are driven by a common North Atlantic hydroclimatic forcing. The persistent quarter-cycle phase lag between the records reflects contrasting system responses rather than chronological discrepancies. While the stalagmite responds rapidly to changes in precipitation, the Angstel/Vecht oak record integrates hydroclimatic forcing over longer timescales through groundwater storage and catchment-

scale hydrological processes. This integrative behaviour results in a quarter-cycle delayed response, demonstrating that lowland wetland trees act as nonlinear biological filters of climate variability.

Our findings underscore that hydroclimate in the Rhine–Meuse delta is shaped by a hierarchy of interacting processes, in which high-frequency atmospheric variability operates within the boundary conditions set by slower oceanic and solar cycles. The Angstel/Vecht record captures both the immediate impacts of extreme hydrological events and the cumulative effects of sustained moisture anomalies, offering a unique perspective on how climate signals are transformed within terrestrial systems. Overall, this work highlights the untapped potential of lowland bog oak archives to reconstruct past hydroclimatic variability and to disentangle the complex interplay of forcing mechanisms across timescales.

7. Data availability

No new data was generated as part of this study.

8. Supplementary material

S1: The R code used in this study can be found at https://github.com/stratigraphy/Weesp-dendro-cycles.

9. References

Adolph, M. L., Czerwiński, S., Dreßler, M., Strobel, P., Bliedtner, M., Lorenz, S., Debret, M., and Haberzettl, T., 2024. North Atlantic Oscillation polarity during the past 3000 years derived from sediments of a large lowland lake, Schweriner See, in NE Germany. Climate of the Past, 20, 2143-2165. https://doi.org/10.5194/cp-20-2143-2024

Ait Brahim, Y., Wassenburg, J. A., Cruz, F. W., Sifeddine, A., Scholz, D., Bouchaou, L., Dassié, E. P., Jochum, K. P., Edwards, R. L., and Cheng, H., 2018. Multi-decadal to centennial hydro-climate variability and linkage to solar forcing in the Western Mediterranean during the last 1000 years. Scientific Reports, 8, 17446. https://doi.org/10.1038/s41598-018-35498-x

Appenzeller, C., Stocker, T. F., and Anklin, M., 1998. North Atlantic Oscillation dynamics recorded in Greenland ice cores. Science, 282(5388), 446-449.

Arts, M., 2023. WaverideR: Extracting Signals from Wavelet Spectra. R package version 0.1.0. Available on CRAN: https://CRAN.R-project.org/package=WaverideR

Arts, M., Corradini, C., Pondrelli, M., Pas, D., and Da Silva, A. C., 2024. Age and orbital forcing in the upper Silurian Cellon section (Carnic Alps, Austria) uncovered using the WaverideR R package. Frontiers in Earth Science, 12, 1357751. https://doi.org/10.3389/feart.2024.1357751

Baker, A., Hellstrom, J., Kelly, B. F. J., Mariethoz, G., and Trouet, V., 2015. A composite annual-resolution stalagmite record of North Atlantic climate over the last three millennia. Scientific Reports, 5, 10307. https://doi.org/10.1038/srep10307

Baker, A., Wilson, R., Fairchild, I. J., Franke, J., Spötl, C., Mattey, D., Trouet, V., and Fuller, L., 2011. High resolution δ18O and δ13C records from an annually laminated Scottish stalagmite and relationship with last millennium climate. Global and Planetary Change, 79, 303-311. https://doi.org/10.1016/j.gloplacha.2010.12.007

Baldini, L. M., McDermott, F., Foley, A. M., and Baldini, J. U. L., 2008. Spatial variability in the European winter precipitation δ18O-NAO relationship: Implications for reconstructing NAO-mode climate variability in the Holocene. Geophysical Research Letters, 35, L04709. https://doi.org/10.1029/2007GL032027

Baldwin, M. P., et al., 2001. The quasi-biennial oscillation. Reviews of Geophysics, 39(2), 179-229.

Bond, G., Kromer, B., Beer, J., Muscheler, R., Evans, M. N., Showers, W., Hoffmann, S., Lotti-Bond, R., Hajdas, I., and Bonani, G., 2001. Persistent solar influence on North Atlantic climate during the Holocene. Science, 294(5549), 2130-2136.

Börgel, F., Frauen, C., Neumann, T., and Markus Meier, H. E., 2020. The atlantic multidecadal oscillation controls the impact of the north atlantic oscillation on north european climate. Environmental Research Letters, 15, 104025. https://doi.org/10.1088/1748-9326/aba925

Bos, I. J., Feiken, H., Bunnik, F., and Schokker, J., 2009. Influence of organics and clastic lake fills on distributary channel processes in the distal Rhine-Meuse delta (The Netherlands). Palaeogeography, Palaeoclimatology, Palaeoecology, 284(3-4), 355-374.

Brehm, N., et al., 2021. Eleven-year solar cycles over the last millennium revealed by radiocarbon in tree rings. Nature Geoscience, 14(1), 10-15.

Brönnimann, S., Franke, J., Valler, V., Hand, R., Samakinwa, E., Lundstad, E., Burgdorf, A. M., Lipfert, L., Pfister, L., Imfeld, N., and Rohrer, M., 2025. Past hydroclimate extremes in Europe

538 driven by Atlantic jet stream and recurrent weather patterns. Nature Geoscience, 18(3),
539 246-253.
540 Brönnimann, S., Malik, A., Stickler, A., Wegmann, M., Raible, C. C., Muthers, S., Anet, J. G.,
541 Rozanov, E. V., and Schmutz, W. K., 2016. Multidecadal variations of the effects of the
542 Quasi-Biennial Oscillation on the climate system. Atmospheric Chemistry and Physics, 16,
543 15529-15543.
544 Brouwer, F., van Delft, S. P. J., and Kemmers, R. H., 2002. Landinventarisatie en ruimtelijke
545 systeemanalyse van het herinrichtingsgebied De Vechtstreek, fase 2; resultaten van een
546 bodemgeografisch onderzoek.
547 Choudhury, S. M., Shah, S. L., and Thornhill, N. F., 2008. Bispectrum and bicoherence. In
548 Diagnosis of Process Nonlinearities and Valve Stiction: Data Driven Approaches, Springer,
549 29-41.
550 Coder, K.D., 1994. Flood damage to trees. University of Georgia Extension, Forest Resources
551 Publication FOR94-61.
552 Cook, E. R., 1990. A conceptual linear aggregate model for tree rings. In Cook, E. R., and
553 Kairiukstis, L. A. (Eds.), Methods of Dendrochronology. Kluwer Academic Publishers,
554 Dordrecht, 98-104.
555 Cook, E. R., D'Arrigo, R. D., and Briffa, K. R., 1998. A reconstruction of the North Atlantic
556 Oscillation using tree-ring chronologies from North America and Europe. The Holocene, 8(1),
557 9-17.
558 Copini, P., den Ouden, J., Robert, E.M.R., Tardif, J.C., Loesberg, W.A., Goudzwaard, L., Sass-
559 Klaassen, U., 2016. Flood-ring formation and root development in response to experimental
560 flooding of young *Quercus robur* trees. **Front. Plant Sci.** 7, 775, 1–14.
561 https://doi.org/10.3389/fpls.2016.00775.
562 De Lange, G. W., and Bles, B., 1963. De bodemgesteldheid rondom de gemeente Weesp:
563 structuurplan Weesp.
564 Delworth, T. L., and Mann, M. E., 2000. Observed and simulated multidecadal variability in
565 the Northern Hemisphere. Climate Dynamics, 16, 661-676.
566 Denniston, R. F., et al., 2018. A stalagmite test of North Atlantic SST and Iberian
567 hydroclimate linkages over the last two glacial cycles. Climate of the Past, 14(12), 1893-
568 1913.

569 Dieppois, B., Durand, A., Fournier, M., and Massei, N., 2013. Links between multidecadal
570 and interdecadal climatic oscillations in the North Atlantic and regional climate variability of
571 northern France and England since the 17th century. Journal of Geophysical Research:
572 Atmospheres, 118, 4359-4372. https://doi.org/10.1002/jgrd.50392
573 Domeisen, D., Badin, G., and Koszalka, I., 2018. How Predictable Are the Arctic and North
574 Atlantic Oscillations? Exploring the Variability and Predictability of the Northern
575 Hemisphere. Journal of Climate, 31, 997-1014.
576 Eade, R., Stephenson, D. B., Scaife, A. A., and Smith, D. M., 2022. Quantifying the rarity of
577 extreme multi-decadal trends: How unusual was the late twentieth century trend in the
578 North Atlantic Oscillation? Climate Dynamics, 58, 1555-1568.
579 Enfield, D. B., Mestas-Nunez, A. M., and Trimble, P. J., 2001. The Atlantic multidecadal
580 oscillation and its relation to rainfall and river flows in the continental US. Geophysical
581 Research Letters, 28, 2077-2080.
582 Faust, J. C., Fabian, K., Milzer, G., Giraudeau, J., and Knies, J., 2016. Norwegian fjord
583 sediments reveal NAO related winter temperature and precipitation changes of the past
584 2800 years. Earth and Planetary Science Letters, 435, 84-93.
585 https://doi.org/10.1016/j.epsl.2015.12.003
586 Folland, C. K., Knight, J., Linderholm, H. W., Fereday, D., Ineson, S., and Hurrell, J. W., 2009.
587 The summer North Atlantic Oscillation: Past, present, and future. Journal of Climate, 22,
588 1082-1103.
589 Goldenberg, S. B., Landsea, C. W., Mestas-Nuñez, A. M., and Gray, W. M., 2001. The recent
590 increase in Atlantic hurricane activity: Causes and implications. Science, 293, 474-479.
591 Geirsdóttir, Á., Miller, G.H., Larsen, D.J. and Ólafsdóttir, S., 2013. Abrupt Holocene climate
592 transitions in the northern North Atlantic region recorded by synchronized lacustrine
593 records in Iceland. Quaternary Science Reviews, 70, 48-62.
594 Gray, S. T., Graumlich, L. J., Betancourt, J. L., and Pederson, G. T., 2004. A tree-ring based
595 reconstruction of the Atlantic Multidecadal Oscillation since 1567 AD. Geophysical Research
596 Letters, 31, L12205.
597 Hagelberg, T., Pisias, N., and Elgar, S., 1991. Linear and nonlinear couplings between orbital
598 forcing and the marine $\delta^{18}O$ record during the Late Neocene. Paleoceanography, 6, 729-746.
599 Hathaway, D. H., 2015. The Solar Cycle. Living Reviews in Solar Physics, 12, 4.
600 https://doi.org/10.1007/lrsp-2015-4

Hathaway, D. H., and Wilson, R. M., 2004. What the Sunspot Record Tells Us About Space Climate. Solar Physics, 224, 5-19.

Holman, I.P., Rivas-Casado, M., Howden, N.J.K., Bloomfield, J.P. and Williams, A.T. (2009), Linking North Atlantic ocean–atmosphere teleconnection patterns and hydrogeological responses in temperate groundwater systems. Hydrol. Process., 23: 3123-3126. https://doi.org/10.1002/hyp.7466

Hijma, M. P., and Cohen, K. M., 2019. Holocene sea-level database for the Rhine-Meuse Delta, The Netherlands: Implications for the pre-8.2 ka sea-level jump. Quaternary Science Reviews, 214, 68-86.

Hubeny, J. B., King, J. W., and Santos, A., 2006. Subdecadal to multidecadal cycles of Late Holocene North Atlantic climate variability preserved by estuarine fossil pigments. Geology, 34, 569-572.

Hurrell, J. W., 1995. Decadal Trends in the North Atlantic Oscillation: Regional Temperatures and Precipitation. Science, 269(5224), 676-679.

Hurrell, J. W., Kushnir, Y., Ottersen, G., and Visbeck, M., 2003. An overview of the North Atlantic oscillation. Geophysical Monograph-American Geophysical Union, 134, 1-36.

Hurrell, J. W., and Van Loon, H., 1997. Decadal variations in climate associated with the North Atlantic Oscillation. Climatic Change, 36, 301-326.

Jansma, E., 2020. Hydrological disasters in the NW-European Lowlands during the first millennium AD: A dendrochronological reconstruction. Netherlands Journal of Geosciences, 99, e11.

Kelly, P. M., Leuschner, H. H., Briffa, K. R., and Harris, I. C., 2002. The climatic interpretation of pan-European signature years in oak ring-width series. The Holocene, 12, 689-694.

Knudsen, M. F., Seidenkrantz, M.-S., Jacobsen, B. H., and Kuijpers, A., 2011. Tracking the Atlantic Multidecadal Oscillation through the last 8,000 years. Nature Communications, 2, 178.

Land, A., Kromer, B., Remmele, S., Brehm, N., and Wacker, L., 2020. Complex imprint of solar variability on tree rings. Environmental Research Communications, 2, 101003.

Leuschner, H. H., Sass-Klaassen and Hanraets, U., Jansma, E., Baillie, M. G. L., and Spurk, M., 2002. Subfossil European bog oaks: Population dynamics and long-term growth depressions as indicators of changes in the Holocene hydro-regime and climate. The Holocene, 12, 695-706.

633 Lohmann, G., Rimbu, N., and Dima, M., 2004. Climate signature of solar irradiance
634 variations: Analysis of long-term instrumental, historical, and proxy data. International
635 Journal of Climatology, 24, 1045-1056.
636 Lüdecke, H., Cina, R., Dammschneider, H., and Lüning, S., 2020. Decadal and multidecadal
637 natural variability in European temperature. Journal of Atmospheric and Solar-Terrestrial
638 Physics, 205, 105294.
639 Luterbacher, J., et al., 2001. Extending North Atlantic oscillation reconstructions back to
640 1500. Atmospheric Science Letters, 2, 114-124.
641 Massei, N., Durand, A., Deloffre, J., Dupont, J.-P., Valdes, D., and Laignel, B., 2007.
642 Investigating possible links between the North Atlantic Oscillation and rainfall variability in
643 northwestern France over the past 35 years. Journal of Geophysical Research: Atmospheres,
644 112, 2005JD007000.
645 Meyers, S. R., 2014. astrochron: A Computational Tool for Astrochronology. R package
646 version 1.6. Available on CRAN: https://CRAN.R-project.org/package=astrochron
647 Meyers, S. R., 2019. Cyclostratigraphy and the problem of astrochronologic testing. Earth-
648 Science Reviews, 190, 190-223.
649 Miyahara, H., Yokoyama, Y., and Yamaguchi, Y. T., 2009. Influence of the Schwabe/Hale solar
650 cycles on climate change during the Maunder Minimum. Proceedings of the International
651 Astronomical Union, 5, 427-433.
652 Murphy, J. O., Sampson, H., Veblen, T. T., and Villalba, R., 1994. Regression Model for the
653 22-year Hale Solar Cycle Derived from High Altitude Tree-ring Data. Publications of the
654 Astronomical Society of Australia, 11, 157-163.
655 Nintcheu-Fata, S., et al., 2003. Chronomics of tree rings for chronoastrobiology and beyond.
656 Biomedicine & Pharmacotherapy, 57, 24-30.
657 Ólafsdóttir, K. B., Geirsdóttir, Á., Miller, G. H., and Larsen, D. J., 2013. Evolution of NAO and
658 AMO strength and cyclicity derived from a 3-ka varve-thickness record from Iceland.
659 Quaternary Science Reviews, 69, 142-154.
660 Olsen, J., Anderson, N. J., and Knudsen, M. F., 2012. Variability of the North Atlantic
661 Oscillation over the past 5,200 years. Nature Geoscience, 5, 808-812.
662 Oz, A., Sen, A., Sancho, C., and Genty, D., 2009. Wavelet analysis of late holocene stalagmite
663 records from ortigosa caves in northern spain. Journal of Cave and Karst Studies, 71.

Pilcher, J. R., Hillam, J., Baillie, M. G. L., and Pearson, G. W., 1977. A long subfossil oak tree-ring chronology from the north of Ireland. New Phytologist, 79, 713-729.

Pinto, J. G., and Raible, C. C., 2012. Past and recent changes in the North Atlantic oscillation. WIREs Climate Change, 3, 79-90.

Poelman, J. N. B., 1966. De bodem van Utrecht: toelichting bij blad 6 van de bodemkaart van Nederland schaal 1:200.000. Stichting voor Bodemkartering, Wageningen.

Proctor, C. J., Baker, A., and Barnes, W. L., 2002. A three thousand year record of North Atlantic climate. Climate Dynamics, 19, 449-454.

Proctor, C. J., Baker, A., Barnes, W. L., and Gilmour, M. A., 2000. A thousand year speleothem proxy record of North Atlantic climate from Scotland. Climate Dynamics, 16, 815-820.

Roig, F. A., Barriopedro, D., García Herrera, R., Patón Dominguez, D., and Monge, S., 2009. North atlantic oscillation signatures in western iberian tree-rings. Geografiska Annaler: Series A, Physical Geography, 91, 141-157.

Rossi, A., Massei, N., and Laignel, B., 2011. A synthesis of the time-scale variability of commonly used climate indices using continuous wavelet transform. Global and Planetary Change, 78, 1-13.

Rust, W., Cuthbert, M., Bloomfield, J., Corstanje, R., Howden, N., and Holman, I., 2020. Exploring the role of hydrological pathways in modulating North Atlantic Oscillation (NAO) teleconnection periodicities from UK rainfall to streamflow. Hydrology and Earth System Sciences, https://doi.org/10.5194/hess-2020-312

Rust, W., Bloomfield, J. P., Cuthbert, M., Corstanje, R., and Holman, I., 2022. The importance of non-stationary multiannual periodicities in the North Atlantic Oscillation index for forecasting water resource drought. Hydrology and Earth System Sciences, 26, 2449-2467.

Sass-Klaassen and Hanraets, U., and Hanraets, E., 2006. Woodlands of the past: The excavation of wetland woods at Zwolle-Stadshagen (the Netherlands). Growth pattern and population dynamics of oak and ash. Netherlands Journal of Geosciences, 85(1), 61-71.

Scaife, A., Folland, C., Alexander, L., Moberg, L.V. Knight, ,. 2008. European Climate Extremes and the North Atlantic Oscillation. Journal of Climate. 21. 72-83. 10.1175/2007JCLI1631.1.

Schlesinger, M. E., and Ramankutty, N., 1994. An oscillation in the global climate system of period 65-70 years. Nature, 367, 723-726.

Schultz, J. A., et al., 2015. Sensitivity of proxies on non-linear interactions in the climate system. Scientific Reports, 5, 18560.

Seidenglanz, A., Prange, M., Varma, V., and Schulz, M., 2012. Ocean temperature response to idealized Gleissberg and de Vries solar cycles in a comprehensive climate model. Geophysical Research Letters, 39, L20702.

Seip, K. L., Grøn, Ø., and Wang, H., 2019. The North Atlantic Oscillations: Cycle Times for the NAO, the AMO and the AMOC. Climate, 7, 43.

Sonett, C. P., and Finney, S. A., 1990. The spectrum of radiocarbon. Philosophical Transactions of the Royal Society of London. Series A, 330, 413-426.

Sonett, C. P., Williams, C. R., and Mörner, N.-A., 1992. The fourier spectrum of Swedish riverine varves: Evidence of sub-arctic quasi-biennial (QBO) oscillations. Global and Planetary Change, 6, 57-65.

Steirou, E., Gerlitz, L., Apel, H., and Merz, B., 2017. Links between large-scale circulation patterns and streamflow in Central Europe: A review. Journal of Hydrology, 549, 484-500.

Sullivan, N. B., et al., 2023. Millennial-scale variability of the Antarctic ice sheet during the early Miocene. Proceedings of the National Academy of Sciences (PNAS), 120(19), e2215036120.

Sutton, R. T., and Hodson, D. L. R., 2005. Atlantic Ocean forcing of North American and European summer climate. Science, 309, 115-118.

Taner, M. T., 2000. Attributes revisited. Technical Publication.

Toonen, W. H. J., Middelkoop, H., Konijnendijk, T. Y. M., Macklin, M. G., and Cohen, K. M. (2016) The influence of hydroclimatic variability on flood frequency in the Lower Rhine. Earth Surf. Process. Landforms, 41: 1266–1275. doi: 10.1002/esp.3953.

Trouet, V., et al., 2009. Persistent positive North Atlantic Oscillation mode during the Medieval Climate Anomaly. Science, 324, 78-80.

Van Asselen, S., Cohen, K. M., and Stouthamer, E., 2017. The impact of avulsion on groundwater level and peat formation in delta floodbasins during the middle-Holocene transgression in the Rhine-Meuse delta, The Netherlands. The Holocene, 27(11), 1694-1706.

Van der Woude, J. D., 1984. The fluviolagoonal palaeoenvironment in the Rhine/Meuse deltaic plain. Sedimentology, 31, 395-400.

Van Dinter, M. V., Cohen, K. M., Hoek, W. Z., et al., 2017. Late Holocene lowland fluvial archives and geoarchaeology: Utrecht's case study of Rhine River abandonment under Roman and medieval settlement. Quaternary Science Reviews, 166, 227-265.

Viviroli, D., Weingartner, R. and Messerli, B., 2003. Assessing the hydrological significance of the world's mountains. Mountain research and Development, 23(1), 32-40.

Vos, P., 2015. Origin of the Dutch coastal landscape: long-term landscape evolution of the Netherlands during the Holocene, described and visualized in national, regional and local palaeogeographical map series. PhD Thesis, Utrecht University.

Vos, P., van der Meulen, M., Weerts, H., and Bazelmans, J., 2020. Atlas of the Holocene Netherlands: Landscape and Habitation since the Last Ice Age. Amsterdam University Press.

Vreugdenhil, S. J., Kramer, K., Pelsma, T., 2006. Effects of flooding duration, -frequency and –depth on the presence of saplings of six woody species in north-west Europe, Forest Ecology Management, vol. 236, 47-55

Wanner, H., et al., 2001. North Atlantic Oscillation-concepts and studies. Surveys in Geophysics, 22, 321-381.

Weerts, H., Cleveringa, P., and Gouw, M., 2002. De Vecht/Angstel, een riviersysteem in het veen. Grondboor & Hamer, 56(3/4), 66-71.

Welch, P. D., 1967. The use of fast Fourier transform for the estimation of power spectra: A method based on time averaging over short, modified periodograms. IEEE Transactions on Audio and Electroacoustics, 15(2), 70-73.